University of Maryland, College Park
Department of Aerospace Engineering

LANGLEY GRANT
IN-02-CR
99264
P. 20

Final Technical Report for NASA Grant NAG-1-681

Studies in General Aviation Aerodynamics

Allen E. Winkelmann
Department of Aerospace Engineering
University of Maryland
College Park, MD 20742

(NASA-CR-190431) STUDIES IN GENERAL AVIATION AERODYNAMICS Final Technical Report (Maryland Univ.) 20 p
N92-28511
Unclas
G3/02 0099264

Final Technical Report for NASA Grant NAG-1-681
Studies in General Aviation Aerodynamics

Introduction

The Department of Aerospace Engineering at the University of Maryland has completed a research study for NASA Langley on the application of drooped leading edges to high aspect wings. The study was supported under NASA Grant NAG-1-681 with Mr. Daniel DiCarlo as grant monitor. Additional support for a graduate student (Hugo A. Gonzalez) was obtained from NASA Headquarters (Underrepresented Minority Focus Program) Grant NTG-70090.

The experimental study conducted for this grant was a natural extension of work previously conducted at NASA Ames, the University of Michigan, NASA Langley and the University of Maryland. Previous research had shown that wing planform modifications (commonly referred to as drooped leading edge mods) could have a significant effect on reducing or eliminating the stall/spin characteristics of General Aviation (GA) aircraft. All aircraft studied in the earlier work had relatively low aspect ratio wings (AR = 6). Since future GA aircraft will feature higher aspect ratio wings, the obvious question was - "how well will the dropped leading edge work on higher aspect ratio wings"? The focus of the current study was to examine the effectiveness of the dropped leading edge modifications to higher aspect ratio wings with AR = 9 to 12.

Research Highlights

The principal results of this study were presented in the following reports:

Gonzalez, H. and Winkelmann, A.E., "Design of a Three-Component Wall-Mounted Balance", AIAA Paper No. 90-1397, Seattle, WA, June 18-20, 1990.

Gonzalez, H., "An Experimental Study of Drooped Leading Edge Modifications on High Aspect Ratio Wings," Master Thesis, Department of Aerospace Engineering, University of Maryland, December, 1991.

Both reports listed above are currently in preparation for submission to the AIAA Journal and the Journal of Aircraft for publication. The first report was presented at the AIAA 16th Aerodynamic Ground Testing Conference held at Seattle, Washington on June 18-20, 1990. A copy of this report is attached. The principle results of this study are summarized in the following (edited) chapter of Mr. Gonzalez's thesis:

Chapter 4: Conclusions and Recommendations

A series of force, moment, and surface flow visualization tests were conducted on reflection plane rectangular wings with NACA 64_2-415 (Modified) and NLF (1) - 0414 airfoil sections and with effective aspect ratios of 6, 9, and 12. The tests were conducted on unmodified (baseline) and modified wings. The modified wings consisted of leading edge gloves which drooped (leading edge droops) below the baseline airfoil leading edge. The leading edge droop span was varied in length. The leading edge extension length was measured from the wing tip to the discontinuity between the leading edge glove and the baseline

The leading edge droop improved the stall characteristics of the NACA 64_2-415 (Modified) wings with greater success than the NLF (1) - 0414 wings. The better performance of the NACA 64_2-415 (Modified) wings may have been attributed to the larger droop leading edge radius over the NLF droop radius. The larger radius allowed for a gentler stall and a large leading edge favorable pressure gradient.

The use of 3/4 span leading edge droop glove lead to the best improvement in stall characteristics. A 3/4 glove span reduced the primary stall of the baseline wing. The loss of lift coefficient at stall was approximately the same for all aspect ratios. Both the NACA 64_2-415 (Modified) and NLF (1) - 0414 wings began to recover lift immediately after stall. However, the amount of lift onaspect ratio. The lower lift recovered by the NLF wings shows the dependence a droop leading edge has on airfoil shape.

The small loss of lift associated with a 3/4 span leading edge droop generated a small $-dC_R/d\alpha$ over a small angle of attack range when compared to a baseline wing. The small negative change in $dC_R/d\alpha$ associated with a 3/4 span droop potentially reduces the divergence of a longitudinal flight path into a spin. Flight path departure is associated with (large) unsymmetrical stall of an aircraft's wing. An unsymmetrical stall causes the stalled wing to roll and yaw due to the lower lift and higher drag - this results in undesired favorable spin conditions. The small change and short duration in $- dC_R/d\alpha$ decreases the lift and drag difference between the stalled and the unstalled wing. The droop leading edge also causes the port and starboard wing panels to stall at the same time. Spin characteristics of the different wing configurations could not be assessed since the force moment data was taken by a static balance.

The rise in lift coefficient after primary stall of a 3/4 span leading edge droop provides a safety margin in which control of an aircraft can be established. After control has been obtained, the aircraft's angle of attack can be reduced.

The lift recovered after initial stall can be attributed to the large leading edge radius of the drooped glove, the discontinuity vortex between the baseline wing and droop, and the large percent of attached flow on the dropped portion. Since 75% of the wing leading edge is covered by the glove, only the inboard 25% of the wing stalls at primary stall while the outer 3/4's of the wing maintained attached flow except for a small region in the trailing edge. The discontinuity between the glove and the baseline wing generates a vortex which keeps the attached and separated flows apart. This vortex generated a "fence" which lets the outer wing panel act as an independent wing without any large contamination of the inboard separated flow. The "fence" vortex also acts as a tip vortex for the outer wing panel which increases its downwash (decreases effective angle of attack). The downwash generated by the discontinuity vortex increases in strength with increasing angle of attack since the pressure gradient between the lower and upper surface increases. Thus, the outer wing panel behaves as a wing with a large leading edge radius which gradually stalls from the trailing edge with increasing angle of attack.

If the physical length between two tip vortices of a plane rectangular wing is increased, the central portion of the wing sees a larger, effective angle of attack than a smaller wing (due to longer distance between the wing center line and the tip vortex). Hence, a large aspect ratio plane rectangular wing stalls earlier than a low aspect ratio wing. The outer droop wing panel experiences the same effect; hence, the secondary stall of a given droop span occurs earlier for higher aspect ratio wings.

Minimum drag for a drooped wing increased a small amount over baseline wing minimum drag. But drag coefficients associated with lift coefficients less than the C_L corresponding to $C_{D,min}$ were substantially larger than baseline wing data. This increase in drag coefficient would provide a smaller range of cruise C_L's.

To extend the secondary stall angle of attack of a high aspect ratio wing with a 3/4 span droop, a second droop which spans 1/2 - 3/4's of the wing droop could be added to the first droop. The second droop would have a larger leading edge radius than the first droop glove. This configuration would generate two vortex "fences" and three independent stall cell regions which in turn would generate a triple hump lift curve. Based on the flow visualization tests, a suggested flow field and wind loading model of a double droop wing at difference angles of attack was proposed.

An interesting observation was made between the NASA results and the date of this study. The best droop results obtained by NASA were with a droop which covered about half of the aircraft span. This configuration also corresponded to a droop glove which spanned 3/4's of the wetted wing surface. This was the same configuration which generated the best results in this thesis. The above results leads one to believe that the droop span should be sized by wetted wing surface span rather than absolute wing span.

The studies carried out in this thesis suggest that a droop configuration does exist which may alleviate stall and longitudinal flight departure for aircraft with high aspect ratio wings. Further studies to determine the effectiveness of a double droop wing and whether a low, middle, or high wing has any effect on drooped wings should be conducted.

AIAA 90-1397

Design of a Three-Component Wall-Mounted Balance

H. Gonzalez and A. Winklemann
Univ. of Maryland
College Park, MD

AIAA 16th Aerodynamic Ground Testing Conference

June 18-20, 1990 / Seattle, WA

AIAA-90-1397

DESIGN OF A THREE-COMPONENT WALL-MOUNTED BALANCE

Hugo A. Gonzalez* and Allen E. Winkelmann†

Department of Aerospace Engineering
University of Maryland
College Park, MD 20742

Abstract

The design and evaluation of a three-component, wall-mounted pyramidal balance for a small wind tunnel is discussed. The balance was designed to measure lift, drag, pitching moment, and angle of attack. The specific design of each component and mathematical models used to design the balance are covered. Balance evaluation consisted of calibration, tare, and interaction analysis.

Nomenclature

b	table width
b_2	flexure height
c	restraint coefficient ($c = 4$ for fixed ends)
D	drag
E	elastic modulus
F	applied force
I	area moment of inertia
K'	sensitivity coefficient in units of load cell signal per interaction load
K	sensitivity coefficient in units of load cell signal per unit load
l	flexure height
L_e	effective flexure link height
L	load table depth (length)
L	lift
M	pitching moment
P	applied load
t	flexure width
x	distance along a load table member
X_1	unknown normal force
X_2	unknown shear force
X_3	unknown bending moment
E	load cell signal
α	angle of attack
σ	stress
μ	Poisson's ratio
ν	coefficient depending on $(b_2/(L\sqrt{c}))$ (Ref. 7)
ρ	radius of gyration $(t/\sqrt{12})$

Subscripts

D	drag
i	i^{th} balance component term
L	lift
M	pitching moment

INTRODUCTION

This paper will discuss the design, fabrication, and testing of a new three-component balance for use in the Aerospace Boundary Layer Tunnel at the University of Maryland. Considering the importance of direct force and moment measurements in wind tunnel testing, it is surprising how little information exists on the design of external balances. The literature available on external balances is small when compared to the amount of information available on sting balances. One explanation may be that many balances are typically custom made by companies which keep their design techniques proprietary. Since little information on external balance design is available, the emphasis of this paper will be on design aspects the authors think are crucial to a three-component, pyramidal wall-mounted balance.

The balance which is described in this paper was designed to be used in semi-infinite wing tests with effective wing aspect ratios up to 12 (Fig. 1). These tests required a balance with the following minimum requirements:

Test Requirements:

- Maximum Lift Force of 458.17 N (103 lbs)
- Maximum Drag Force of 240.20 N (54 lbs)
- Maximum Pitching Moment of 915.18 N·cm (81 in·lb)
- Maximum Angle of Attack Range from -30° to 60°
- Motorized Angle of Attack Positioning
- Capability of Withstanding a 26483.6 N·cm (2344 in·lb) Combined Rolling Moment and Yawing Moment

The new balance was based on an existing three-component balance in the Aerospace Laboratories at the University of Maryland which could not meet the minimum test requirements. This existing balance was similar in design to a balance used by the staff of the High Speed Laboratory, National Aeronautical Establishment of Canada.[1] Additional references used in designing the new balance were Refs. 2 through 5.

---

* AIAA Student Member, Graduate Student, phone (301)454-2922

† AIAA Member, Associate Professor, phone (301)454-2414

BALANCE DESIGN

Figure 2 shows the basic operating principle of a wall-mounted pyramidal balance. Lift and drag are measured directly from two perpendicular load tables which are aligned parallel to the flow. Pitching moment is read about the balance resolving center. The lift, drag, and pitching moment resolving forces are transmitted to load cells using flexure links.

Based on the resolving and operating system of a pyramidal balance, the design of the balance was divided into five segments:

- **Load Table-** designed to deflect in the lift and drag planes.
- **Cylindrical Core-** designed to hold the model, set the angle of attack, and transmit pitching moment.
- **Motor and Angle Measuring Base-** designed to set and measure angle of attack.
- **Flexure Links-** designed to transmit deflections to load cells.
- **Load Cells-** measure lift, drag, and pitching moment.

Figures 3 and 4 show a cross-sectional view of the balance and a photograph of the assembled balance.

Load Table Design

A load table responds to a force by deflecting in the direction of the force (as shown in Fig. 5), but resists movement in other directions. As shown in Fig. 6, with the load tables lined up with the wind axis, the lift load table moves vertically, while the drag load table moves horizontally. To accomplish this, the load tables need to be supported on very thin flexures. The drag flexure assembly is mounted directly to the base of the balance, while the lift table assembly rides on top of the drag table. The lift load cell is attached to the test section wall and essentially helps support the weight of the balance (along with the drag flexures). Using the lift load cell to help support the balance allows one to use very thin lift and drag flexures for tests at low speed and low angle of attack. Any balance interactions caused by this arrangement can readily be accounted for in computer processing of the data.

With a thin flexure, one must consider the danger of buckling under compressive loads created by rolling and yawing moments produced by lift and drag. To determine flexure size, two mathematical models were used: the Unit Load Method to predict deflection[6] and a Plate Column Model to predict buckling[7].

Deflection analysis based on the unit load method and nomenclature of Fig. 7 resulted in Eqs. 1 and 2. A series of calculations to determine load table deflection (q), using Eqs. 1 and 2, were completed for a series of flexures 19.05 cm long with varying thicknesses and heights.[8]

$$\begin{bmatrix} \left(\frac{b^3}{3I_2}+\frac{lb^2}{I_1}\right) & \left(\frac{-lb^2}{2I_2}-\frac{l^2b}{2I_1}\right) & \left(\frac{b^2}{2I_2}+\frac{lb}{I_1}\right) \\ \left(\frac{-lb^2}{2I_2}-\frac{l^2b}{2I_1}\right) & \left(\frac{l^2b}{I_2}+\frac{2l^3}{I_1}\right) & \left(\frac{-lb}{I_2}-\frac{l^2}{I_1}\right) \\ \left(\frac{b^2}{2I_2}+\frac{lb}{I_1}\right) & \left(\frac{-lb}{I_2}-\frac{l^2}{I_1}\right) & \left(\frac{b}{I_2}+\frac{2l}{I_1}\right) \end{bmatrix} \begin{bmatrix} X_1 \\ X_2 \\ X_3 \end{bmatrix} \tag{1}$$

$$= \begin{bmatrix} \left(\frac{ab^2}{2I_2}+\frac{alb}{I_1}+\frac{l^2b}{2I_1}\right) \\ -\left(\frac{alb}{I_2}+\frac{al^2}{2I_1}+\frac{l^3}{6I_1}\right) \\ \left(\frac{ab}{I_2}+\frac{al}{I_1}+\frac{l^2}{2I_1}\right) \end{bmatrix} F$$

$$q = \frac{1-\mu^2}{EI_1}\left[\frac{-l^2}{2}X_3 + \frac{l^3}{6}X_2 - \frac{l^2b}{2}X_1 + \left(\frac{al^2}{2} + \frac{l^3}{3}\right)F\right] \tag{2}$$

Flexure buckling was of major concern since the resulting rolling and yawing moments put the flexures under compressive and tensile loads. Figure 8 depicts flexure loading due to a rolling moment. To determine the critical buckling loads, the flexures were modeled as fixed end plate columns. Using Eq. 3, several calculations were carried out by assuming a column length of 19.05 cm and varying the flexure height and width. Tension was not of great concern since buckling occurs before yield.

$$\sigma_{cr} = \frac{v}{1-\mu^2}\,\frac{\pi^2 E}{\left(\frac{L}{\rho\sqrt{c}}\right)^2} \tag{3}$$

The resulting deflection and buckling calculations suggested that a flexure with a 0.051 cm web (plate column thickness) and a height of 4.445 cm was required. As a safety factor against buckling, the web was reinforced at the center, as shown in Fig. 9, and elongated to 21.59 cm. A web reinforcement reduces the effective height of the plate column making it more stable against buckling. Two reinforced flexures were manufactured and tested for deflection and buckling under expected load conditions. Although the flexures had web reinforcements, they closely followed the calculated deflection of unreinforced flexures as shown in Fig. 10. Buckling calculations were validated by applying a 444.82 N load with a moment arm of 65.405 cm. The flexures showed no sign of buckling, even when the load swayed slightly from side to side.

Cylindrical Core Assembly

For design purposes, as depicted in Fig. 3, the cylindrical core assembly was divided into six parts: 1) sting sleeve, 2) sleeve housing, 3) turntable base, 4) turntable, 5) pitching moment arm, and 6) collars. A model is mounted in the balance through the cylindrical core assembly. As a result, the cylindrical core assembly must provide good model alignment and be able to withstand all aerodynamic forces which are transmitted through the sting (mounting shaft). The cylindrical core assembly must also be able to change the model angle of attack either manually or mechanically.

The main concern in designing the cylindrical assembly was the sting sleeve bearing spacing required for model alignment. An additional concern was the ability of the bearings to withstand large rolling and yawing moments encountered when testing high aspect ratio wings with flaps. The importance of model alignment is shown in Fig. 11 and explained below. Consider a bearing misalignment of 0.005 cm (which would be the typical machining tolerance for this piece) and bearing spacings of 2.54, 15.24, and 20.32 cm. For point A, which is 111.76 cm from the left bearing (distance to the tip of a 91.44 cm wing), the corresponding deflections due to a .005 cm bearing misalignment are 0.223, 0.037, and 0.028 cm. This indicates that a separation of 15.24 to 20.32 cm would produce a relatively small induced dihedral or yaw angle compared to the dihedral and yaw angle caused by model deflection during tests. The bearings mounted in the sleeve housing (MPB-3TKCR29-36) have a maximum allowable radial load of 4049 N. This indicated a minimum spacing of 13.08 cm for the bearings to withstand the expected maximum rolling moment of 26483.6 N·cm. The final bearing spacing was 17.15 cm after considering other design aspects such as providing clearance between the lift load cell and motor base, and clearance between the motor and wind tunnel wall.

Although Ref. 4 cautions against the use of bearings in balances, the authors believe that the use of bearings is a viable option provided that the radial force on the bearings is kept well below the manufacturer's specified maximum radial force. Moreover, hysteresis effects due to the bearings may be reduced by wind tunnel shaking and wing flutter. The use of ball bearings (to provide the very small rotational deflection needed for the pitching moment load cell to respond) leads to a relatively simple mechanical design when compared with a design using flexures. Ball bearings have been used previously in a number of different balance designs, as noted in Refs. 1, 2, and 3.

As shown in Fig. 3, the sleeve housing holds the sting sleeve and turntable base. The sting is held in place with two collars which are attached to the sting sleeve. A maximum sting diameter of 3.16 cm was incorporated into the design to allow for pressure lines for boundary layer control, circulation control, and surface pressure measurement tests. As shown in Fig. 12, the pitching moment arm on the sting sleeve is connected to a load cell on the turntable via a flexure link. This allows the turntable to set the model angle of attack. To change or hold angle of attack, the turntable is connected to a stepper motor through a plastic cable chain, as shown in Fig. 13.

The turntable and its base were designed such that the turntable would rotate freely. This was accomplished by housing a pin roller bearing in the base plate, which mates with the turntable hub. The turntable diameter was based on the ability of a stepper motor, with a holding torque of 105.92 N·cm, to support a 915.18 N·cm pitching moment. To prevent the turntable from wobbling, a raceway for 0.3175 cm steel balls was cut into the turntable and baseplate at a radius of 8.255 cm. The depth of the raceway provides a 0.079 cm spacing between the turntable and baseplate. The turntable is held in place by teflon covered ball bearings, as shown in Fig. 3. The teflon tires are used to prevent the steel bearing from cutting into the aluminum.

Motor and Angle Measuring Base

The motor and angle measuring base was designed to serve as a mounting platform for a stepper motor, a 1K ohm 10-turn potentiometer, and a sprocket ratioing system as shown in Fig. 14. ASuperior Electric M093-FC11 stepper motor with a holding torque of 31.777 N·cm was attached to the turntable and sprocket ratioing system through a William Berg Co.

Flex-E-Pitch 25CCF plastic cable chain. To increase the effective holding torque of the motor, a large turntable to motor sprocket ratio was used (10.05:1). A sprocket ratioing system which links the turntable and potentiometer via the Flex-E-Pitch and a Min-E-Pitch 3CCF plastic cable chain was needed to use the full range of the 10-turn potentiometer. The effective rotation ratio of potentiometer to turntable is 38.6 potentiometer turns/turntable turn. This gives 9.65 potentiometer turns for a 90° angle sweep.

Flexure Links

As shown in Figs. 3 and 4, flexure links are used to transmit load table and pitching moment arm deflections to the load cells. Flexure links are designed to be strong in tension but weak in bending - if a flexure link transmits a bending moment to the load cell, an erroneous measurement will result. A review of flexure links used in Refs. 1, 2, and in the Glenn L. Martin Wind Tunnel at the University of Maryland suggested a flexure column height to width ratio of 6 to 1. A 6:1 (0.952 cm to 0.158 cm) ratio proved to be adequate for lift and drag but not for pitching moment, where the resolving force was considerably less. The pitching moment link was modified to a 32:1 height to width ratio (2.54 cm to 0.0794 cm) with a reinforced center. To prevent flexure link buckling and deformation, the flexure links were placed in tension when loaded in positive lift, drag, and negative pitching moment. Critical buckling load calculations were based on Eq. 4.[9] The flexure links were machined from a single piece of 8-32 stainless steel threaded rod.

$$P_{cr}=\frac{\pi^2 EI}{L_e^2} \tag{4}$$

Load Cells

The load cells used in the balance were Interface MB-150, MB-75, and MB-50 strain gage, cantilever beam load cells. The specified accuracy of the three load cells is 0.03% of the rated output. Load cell accuracy was based on the maximum width of the error band of data scatter from a load cell calibration curve. The data scatter band includes nonlinearity, hysteresis, and nonrepeatability.[10] Load cell specifications are summarized in Table 1.

	MB-50	MB-75	MB-150
Rated Capacity Newtons	222	333	666
Accuracy % Rated Output	0.03	0.03	0.03
Deflection at Rated Capacity	0.010 cm	0.010 cm	0.013 cm
Temp. Range Compensated	-15°to 65° Celsius	-15°to 65° Celsius	-15°to 65° Celsius
Temp. Effect on Rated Output- % of Reading/55.6°C	0.08	0.08	0.08

Table 1 Load Cell Specifications

BALANCE FABRICATION

The entire balance was machined out of 6061-T6 aluminum, except for the sting sleeve and collars which were made out of carbon steel. The sting sleeve was made of steel to minimize balance deformation. The lift and drag flexures were machined out of a single piece of aluminum to prevent mechanical slippage under compressive and tensile loads.

BALANCE ELECTRONICS

Figure 15 shows a schematic of the electronic equipment used with the balance. The stepper motor was powered by a Superior Electric SP153B preset indexer. Measurements Group 2310 amplifiers were used to power and amplify load cell signals. The angle of attack potentiometer was powered by a 9.5 volt power supply. Voltmeters were used to monitor the amplifiers, potentiometer, and power supply output. Load and angle of attack readings were processed by a DSP A/D converter and an HP-1000, A900 computer.

BALANCE EVALUATION

To evaluate the balance, a series of angle of attack, lift, drag, pitching moment, and tare calibrations were conducted. Tare calibrations consisted of sweeping the balance with and without a model through an angle of attack range (with wind off) to determine gravitational effects.

The angle of attack, lift, drag, and pitching moment calibrations were linear, repeatable, and showed no hysteresis (see Figs. 16, 17, 18, and 19). When in use, the overall balance/data acquisition system is calibrated before and after each test to assure that any drift in the overall system can be taken into account. Although the long term calibration stability of the balance has not been assessed, the calibration curves obtained each day during tests lasting several weeks were very similar. The small variations that were noted were attributed to drift in the data acquisition system. The basic calibration results showed that there is no mechanical slippage in the load tables, cylindrical core assembly, or the angle of attack positioning/measuring system. However, a change in angle of attack due to a negative pitching moment was encountered. The change in angle of attack is attributed to the stretching of the Flex-E-Pitch chain. Equation 5, based on calibration tests, relates the change in angle of attack to the pitching moment.

$$\alpha = -1.457\times10^{-3} M^2 + 6.263\times10^{-2} M \tag{5}$$

α in degress
M in N·cm

The sensitivity of the balance under the maximum loading conditions are listed in Table 2.

Component	Maximum Load	Sensitivity
Lift	458.2 N	0.0549 N
Drag	240.2 N	0.0186 N
Pitching Moment	915.2 N·cm	0.112 N·cm

Table 2 Balance Sensitivity

Tare calibrations were conducted with and without a wing to determine the offset corrections to be made to the pitching moment data. Tare offsets are due to small pitching moments produced by the weight of the wing. The center of gravity of the wing moves relative to the balance resolving center during an angle of attack sweep.

Figure 20 shows the balance pitching moment tare without a wing. The slight curvature in the plot is due to the moment arm center of gravity following a circular path. The hysteresis loop may be attributed to mechanical run-out between the turntable and turntable base and to hysteresis in the bearings used to support the sting sleeve housing. If the balance had not been used for several days, the initial tare curve was shifted slightly on the plot. However, after an initial angle of attack sweep, a repeat of the calibration showed the same tare curve as obtained in previous tests. This effect was apparently due to a slight "sticking" of the bearings that set in after a number of days. Preliminary tests to evaluate hysteresis in the bearings when a large lift force is placed on the balance indicates a similar tare curve with the hysteresis loop opening up by a factor of two or three. However, since this effect is repeatable a correction for it can be made in data processing.

Figure 21 shows the balance pitching moment tare with a wing. The pitching moment data follows a cosine curve, which corresponds to the wing center of gravity following a circular path. A small hysteresis loop in Fig. 21 is apparent between 0 N·cm and 6.8 N·cm (0 to .6 in·lb).

Balance Interactions

As noted in Ref. 4, no balance is free of interactions. Balance interactions are both linear and nonlinear. Linear interactions (first order) are caused by machining tolerances and component misalignment. Second order nonlinear interactions are due to the elastic deformations that modify the geometry of a balance under load. Plastic deformation of balance parts produce nonlinear third order interactions. If plastic deformation is encountered, then a balance has been improperly designed.[4]

In the case of a three-component balance, the output signal E_i of each load cell is a function of all three components (e.g. L, D, and M). An expression for E_i which includes all first and second order interactions is given as Eq. 6. The equation for the drag load cell signal (i = D) is given as Eq. 7. The subsequent discussion will be limited to the drag load cell signal. The other component signals are evaluated similarly.

$$\begin{aligned} E_i &= K'_{i,L} L + K'_{i,D} D + K'_{i,M} M \\ &+ K'_{i,LL} L^2 + K'_{i,DD} D^2 + K'_{i,MM} M^2 \\ &+ K'_{i,DL} LD + K'_{i,DM} DM + K'_{i,LM} LM \end{aligned} \tag{6}$$

$$\begin{aligned} E_D &= K'_{D,L} L + K'_{D,D} D + K'_{D,M} M \\ &+ K'_{D,LL} L^2 + K'_{D,DD} D^2 + K'_{D,MM} M^2 \\ &+ K'_{D,DL} LD + K'_{D,DM} DM + K'_{D,LM} LM \end{aligned} \tag{7}$$

The sensitivity coefficients K' in Eqs. 6 and 7 have units of load cell output signal per unit of interactive load. The principal sensitivity coefficient for the drag load cell is $K_{D,D}$; the other coefficients represent interactions. This creates three first order and six second order sensitivity coefficients per component, as listed in Table 3.

linear first order	nonlinear second order
$K'_{D,L}$	$K'_{D,LL}$
$K'_{D,D}$	$K'_{D,DD}$ $K'_{D,DL}$
$K'_{D,M}$	$K'_{D,MM}$ $K'_{D,LM}$ $K'_{D,DM}$

Table 3 Linear and Nonlinear Sensitivity Coefficients For the Drag Signal

An interaction calibration was conducted to obtain the K' coefficients. The calibration consisted of the loading configurations listed in Table 4 and explained below. This loading procedure closely followed the technique described in Ref. 11. The balance was first loaded in pure lift or drag in five equal intervals to the maximum expected load. When calibrating for pitching moment, a small secondary load ($L_{max}/10$) was moved along a moment arm to produce a range of pitching moments from 0 to M_{max}. This secondary load resulted in loading the balance in a small, but constant negative lift. For combined loads such as LD, the secondary load L_{max} is held constant while the primary load is varied from 0 to D_{max} in 5 equal increments.

Term Being Evaluated	Primary load added (5 increments)	Secondary load added (constant)
L, L^2	L	None
D, D^2	D	None
M, M^2	M	$L_{max}/10$
LD	D	L_{max}
LM	M	$L_{max}/10$, L_{max}
DM	M	$L_{max}/10$, D_{max}

Table 4 Loading Configurations

The drag signal data from each of the three primary loading tests (L, D, and M) were used to get the K' coefficients generally referred to as the first order and quadratic coefficients. For example, the drag signal data obtained in the pure lift calibration were plotted against lift and fitted to a second order polynomial. The coefficients of this polynomial correspond to $K'_{D,L}$ and $K'_{D,LL}$.

The cross product coefficients such as $K'_{D,DM}$ were also obtained by plotting the drag signal data against the quantity that was varied in the calibration. The data were fitted to a straight line and the cross product coefficient K' was obtained from the slope of the line (1st order coefficient). For example, in the case of the drag and pitching moment cross product (DM), the slope is E_{DM}/M_{max} (where E_{DM} is the small voltage contribution to E_D due to the DM interaction). E_{DM}/M_{max} was divided by D_{max} to obtain $K'_{D,DM}$ as given by Eq. 8.

$$K'_{D,DM} = \frac{E_{DM}}{D_{max} M_{max}} \tag{8}$$

$$= \frac{1^{st}\ \text{Order Coefficient} * M_{max}}{D_{max} M_{max}}$$

To obtain D in terms of engineering units, Eq. 7 was divided by the principle sensitivity coefficient $K'_{D,D}$ which is in units of load cell signal per unit load. The final result for D is given in Eq. 9. The corresponding expressions for L and M are given in Eqs. 10 and 11. Eqs. 9, 10, and 11 cannot be solved directly because the loads appear on both sides of the equations. Instead, an iterative technique is required where the initial or raw data for L, D, and M are used to start the calculations.[4] The sensitivity coefficients for the balance in this paper are summarized in Table 5.

$$\begin{aligned} D = \frac{E_D}{K'_{D,D}} &- K_{D,L} L - K_{D,M} M \\ &- K_{D,LL} L^2 - K_{D,DD} D^2 - K_{D,MM} M^2 \\ &- K_{D,DL} LD - K_{D,DM} DM - K_{D,LM} LM \end{aligned} \tag{9}$$

$$\begin{aligned} L = \frac{E_L}{K'_{L,L}} &- K_{L,D} D - K_{L,M} M \\ &- K_{L,LL} L^2 - K_{L,DD} D^2 - K_{L,MM} M^2 \\ &- K_{L,DL} LD - K_{L,DM} DM - K_{L,LM} LM \end{aligned} \tag{10}$$

$$M = \frac{E_M}{K'_{M,M}} - K_{M,L} L - K_{M,D} D$$

$$-K_{M,LL} L^2 - K_{M,DD} D^2 - K_{M,MM} M^2 \qquad (11)$$

$$-K_{M,DL} LD - K_{M,DM} DM - K_{M,LM} LM$$

	L	D	M
$K_{i,L}$		1.78×10^{-2}	1.85×10^{-2}
$K_{i,D}$	-5.07×10^{-3}		-3.56×10^{-2}
$K_{i,M}$	-1.39×10^{-4}	-2.48×10^{-3}	
$K_{i,LL}$	1.95×10^{-5}	-3.23×10^{-6}	-4.83×10^{-5}
$K_{i,DD}$	-8.42×10^{-6}	1.52×10^{-4}	3.70×10^{-5}
$K_{i,MM}$	4.82×10^{-7}	1.14×10^{-5}	-1.78×10^{-5}
$K_{i,DL}$	8.94×10^{-5}	3.88×10^{-4}	-7.58×10^{-4}
$K_{i,LM}$	4.07×10^{-6}	-2.88×10^{-5}	5.02×10^{-4}
$K_{i,DM}$	3.28×10^{-5}	1.35×10^{-5}	1.96×10^{-4}

Table 5 Interaction Coefficients

CONCLUSION

This paper has discussed the design of a new three-component wall mounted pyramidal balance. The balance was specifically designed for testing high aspect ratio wings with flaps. In addition, the balance has been configured to allow future work with high C_L, boundary layer control, and circulation control models. The balance may be modified for low angle of attack and low Reynolds number tests by changing the load cells and reducing flexure thickness. The specifications for the balance described in this paper are:

- Maximum Lift of 667.23 N (150 lbs)
- Maximum Drag of 333.62 N (75 lbs)
- Maximum Pitching Moment of 3186.1 N·cm (282 in·lb)
- Angle of Attack Range from -30° to 60°
- Capability to Withstand a 26483.6 N·cm (2344 in·lb) Rolling and Yawing Moment

ACKNOWLEDGEMENTS

The authors wish to extend a special note of thanks to: Kevin Bruestle, Victor Hwang, Ian Matlick, Paul Vieira, Taylor Hale, Dan Skane, and the University of Maryland Physics shop for the hard work in helping complete this project. This work was sponsored by NASA Langley Research Center grant No. NAG-1-681 and NASA Headquarters (Underrepresented Minority Focus Program) grant No. NTG-70090.

References

1. "Development of Half-Model Wind Tunnel Balance", AGARD report 10, February 1956.
2. Lambourne, N. C.; "A Note On a Half-Model Strain-Gage Balance", AGARD report 11, February 1956.
3. Huber, Arthur F., II; "Airfoil Moment Coefficients at Low Reynolds Numbers: The Design, Fabrication, and Testing of a Simple Torquemeter", AIAA Midwest Region Student Conference, March 1985.
4. Rae, William H., Jr. and Pope, Alan; Low-Speed Wind Tunnel Testing, John Wiley & Sons, New York, 1984, pp. 152-161.
5. Bardowicks, H.; "A New Six-Component Balance and Applications on Wind Tunnel Models of Slender Structures", Journal of Wind Engineering and Industrial Aerodynamics, Vol. 16, No. 2, April 1984.
6. Allen, David H. and Haisler, Walter E,; Introduction to Aerospace Structural Analysis, John Wiley & Sons, New York, 1989, pp. 307-311.
7. Houbolt, John C. and Stowell, Elbridge Z.; "Critical Stress of Plate Columns", NACA TN-2163, August 1950.
8. Gonzalez, Hugo A.; "An Experimental Study of Droop Leading Modifications on High Aspect Ratio Wings", Masters Thesis, University of Maryland (pending).
9. Beer, Ferdinand P. and Johnston, E. Russell; Mechanics of Materials, McGraw Hill Book Company, New York, 1981.
10. Interface Pamphlet 12-10G, 1985.
11. Hausen, Raymond M.; "Evaluation and Calibration of Wire-Strain-Gage Wind Tunnel Balances Under Load", AGARD report 13, February 1956.
12. Dubois, M.; "Six-component Strain-Gage Balance for Large Wind Tunnels", Proceedings of the Fourth SESA International Congress on Experimental Mechanics, Boston, May 25-30, 1980.
13. Dubois, M.; "Calibration of Aerodynamic Dynamometers and Balances at the Modane-Avrieux Test Center", Presented at the Mesucora Congress, Paris, April 17-21, 1967, (N68-32016).

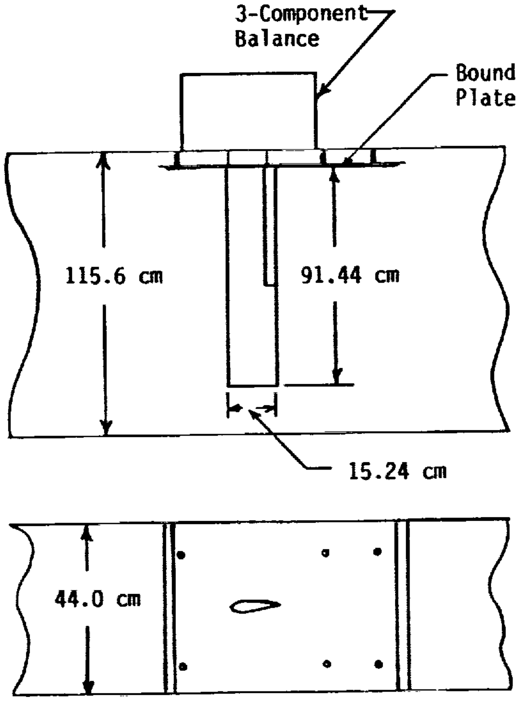

Fig. 1 Wind Tunnel Set-Up

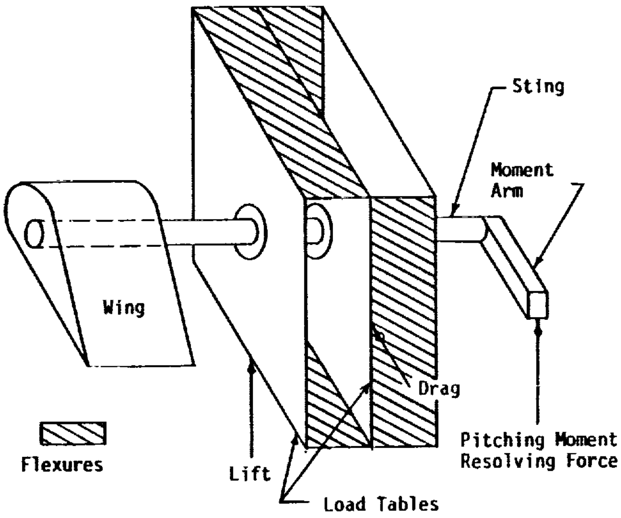

Fig. 2 Pyramidal Balance Resolving System

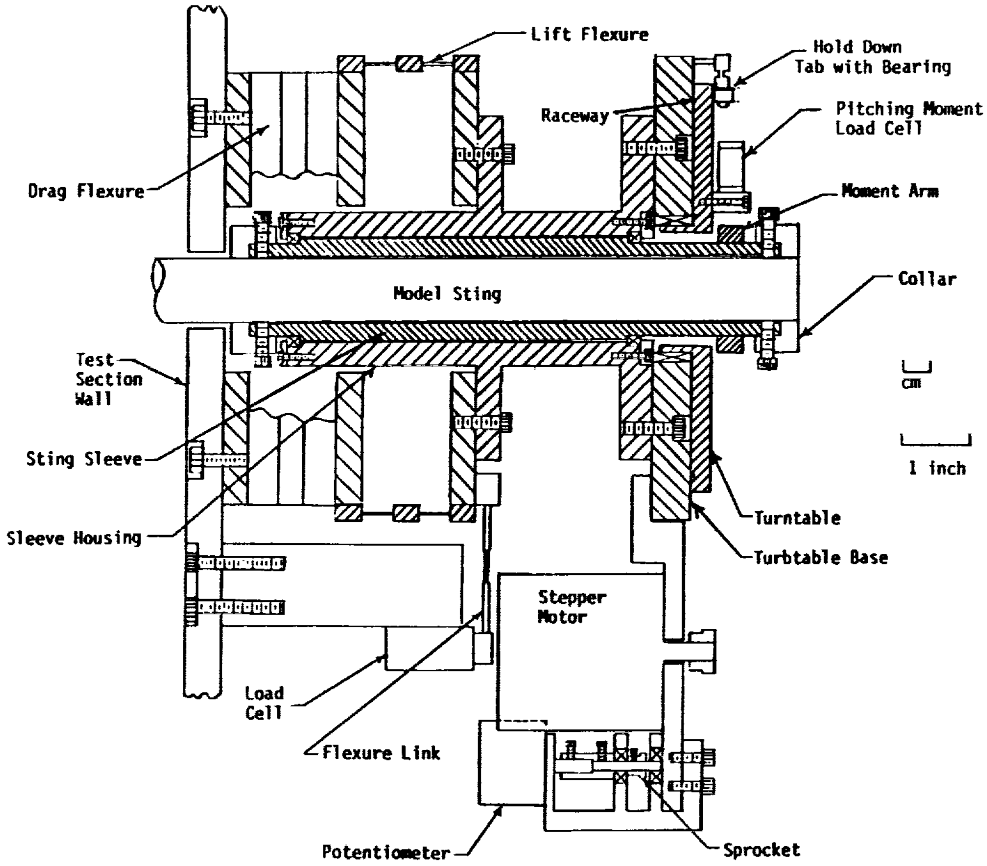

Fig. 3 Cross Sectional View of Balance

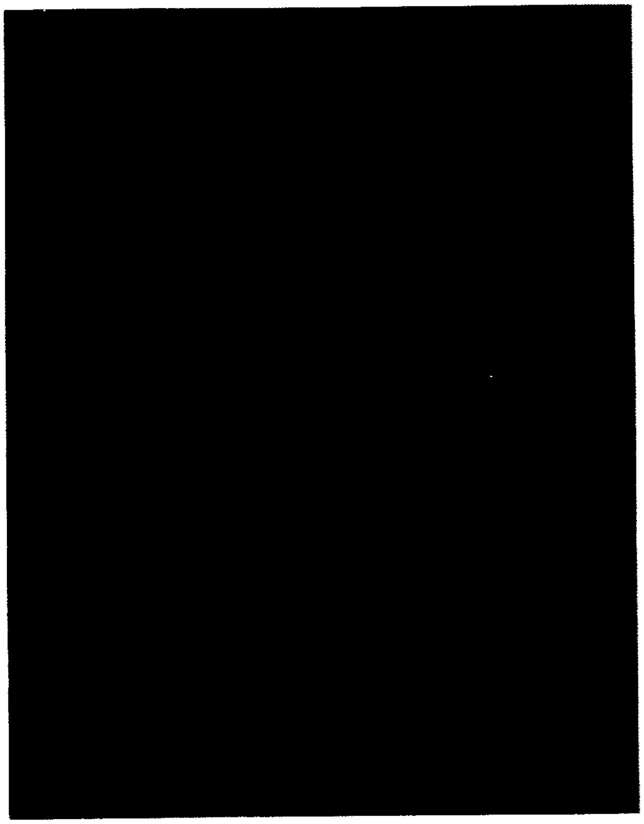

Fig. 4 3-Component, Wall-Mounted, Pyramidal Balance

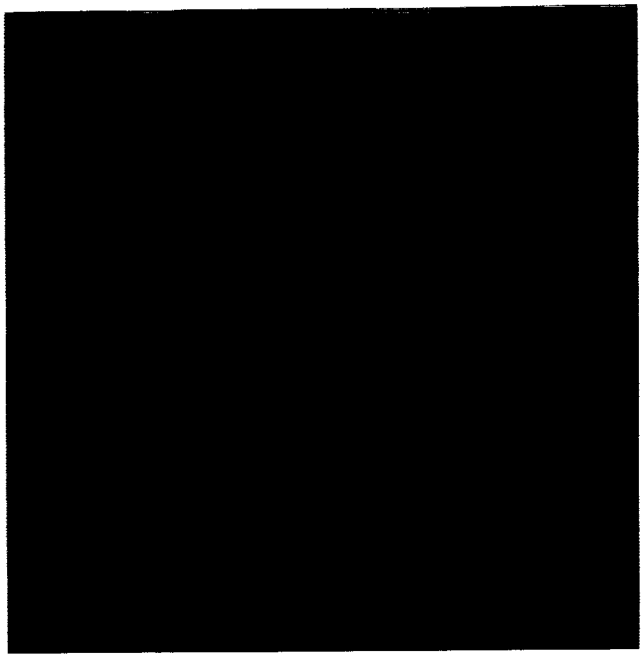

Fig. 6 Load Tables

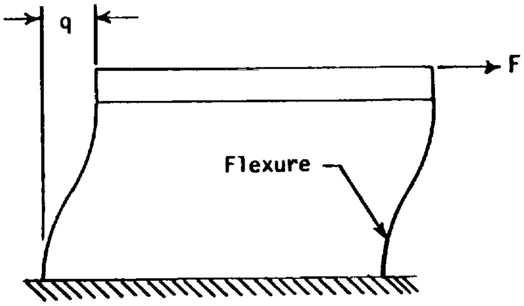

Fig. 5 Load Table Deflection

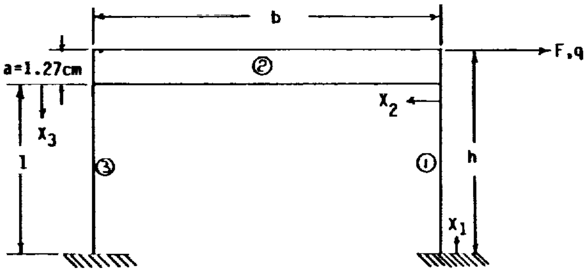

Fig. 7 Unit Load Method Nomenclature

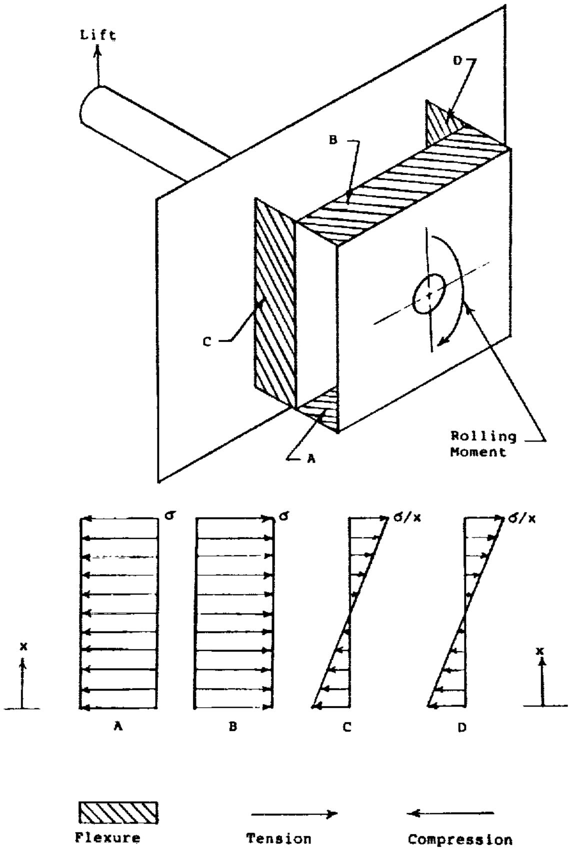

Fig. 8 Flexure Loading Due To Rolling Moment

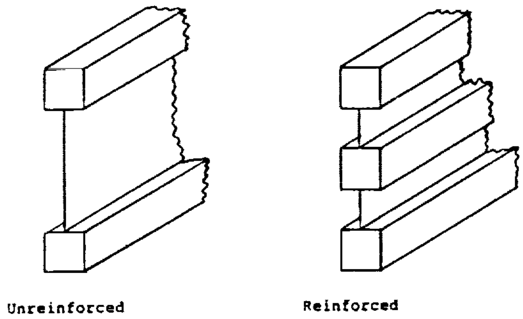

Fig. 9 Unreinforced and Reinforced Flexures

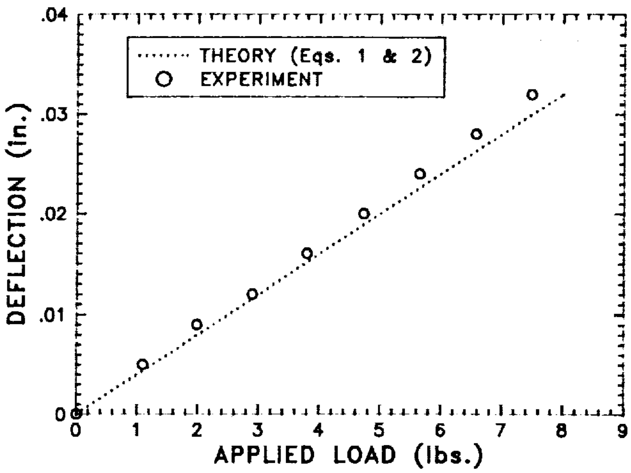

Fig. 10 Load Table Deflection

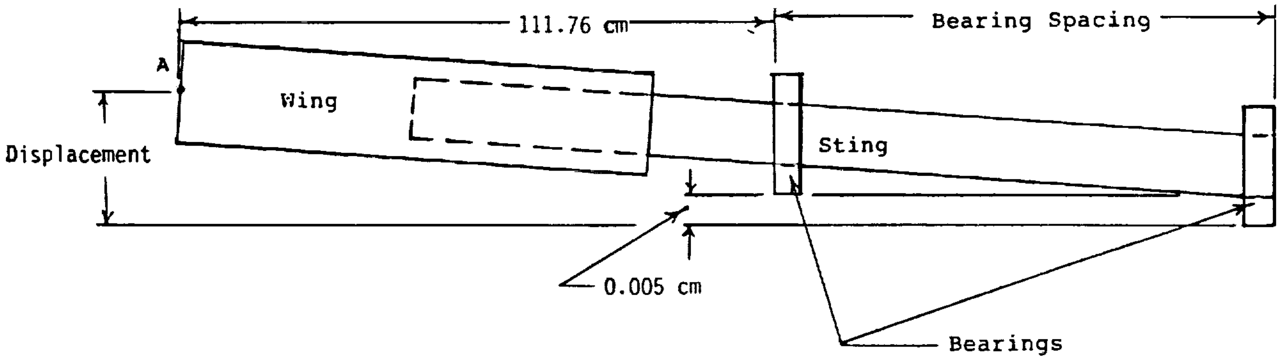

Bearing Spacing	Displacement
2.54 cm	0.223 cm
15.24 cm	0.037 cm
20.32 cm	0.028 cm

Fig. 11 Model Alignment Example

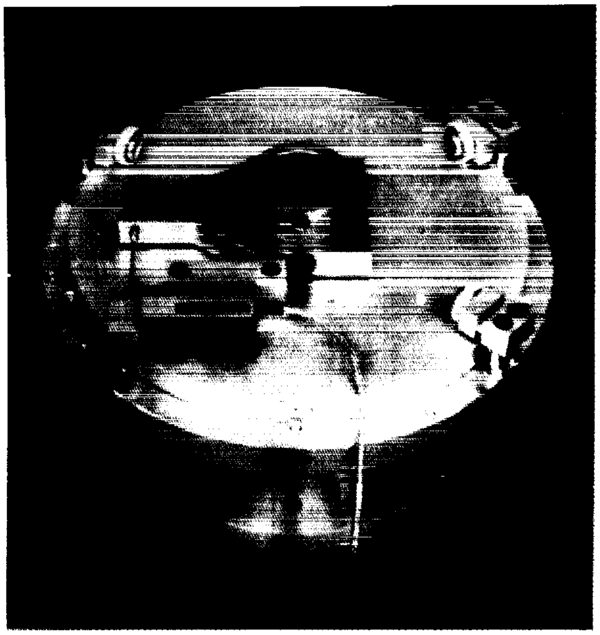

Fig. 12 Balance Cylindrical Core with Load Cell and Flexure Link

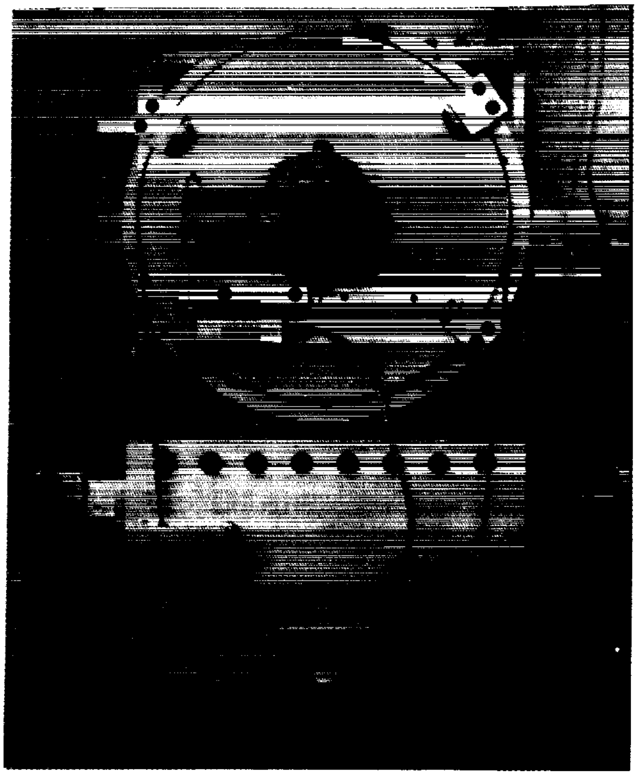

Fig. 13 Turntable/Motor and Angle Measuring Base Set-Up

ORIGINAL PAGE
BLACK AND WHITE PHOTOGRAPH

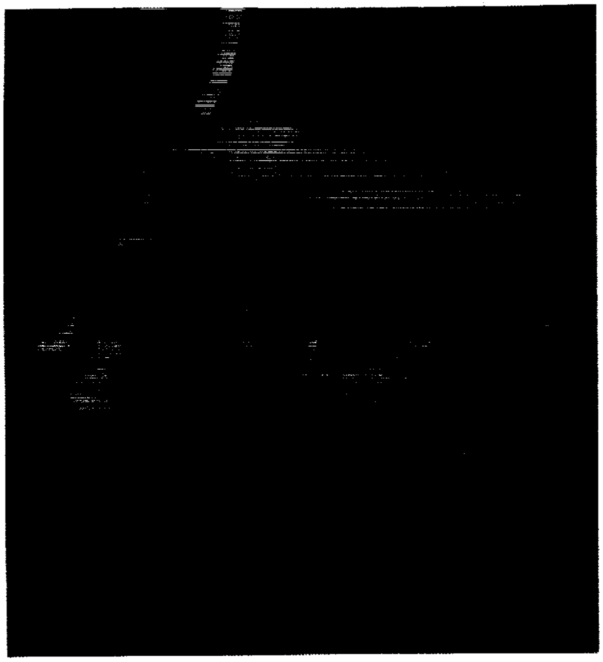

Fig. 14 Motor and Angle Measuring Base

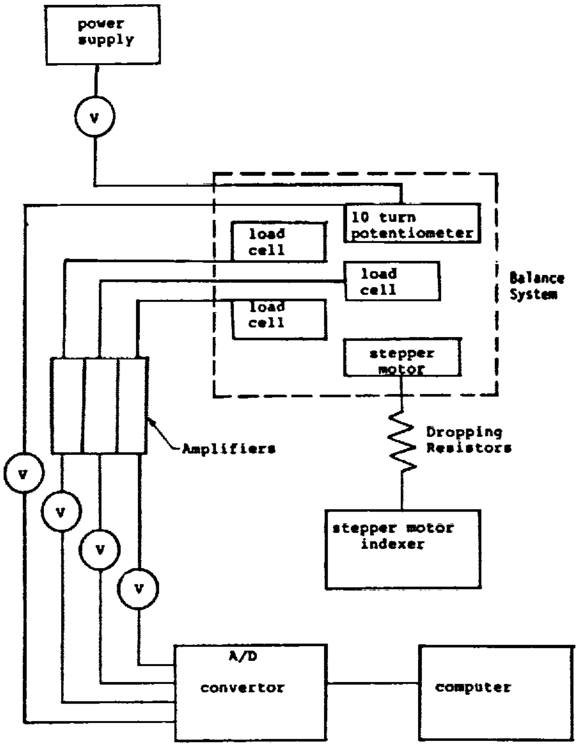

Fig. 15 Balance Electronics Set-Up

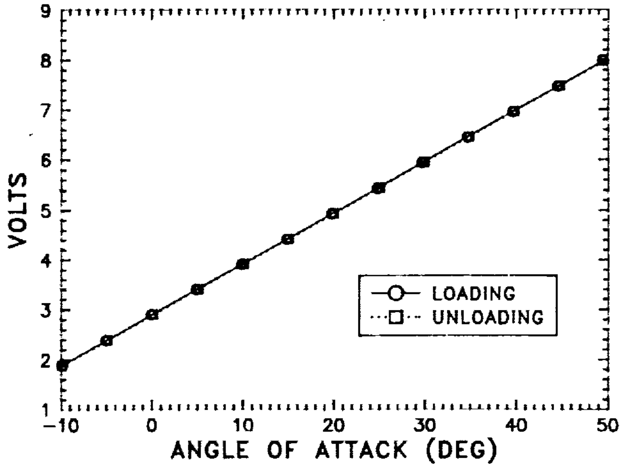

Fig. 16 Angle Calibration

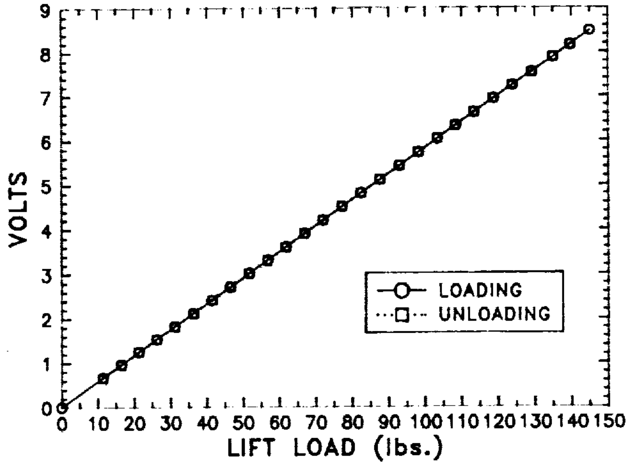

Fig. 17 Lift Calibration

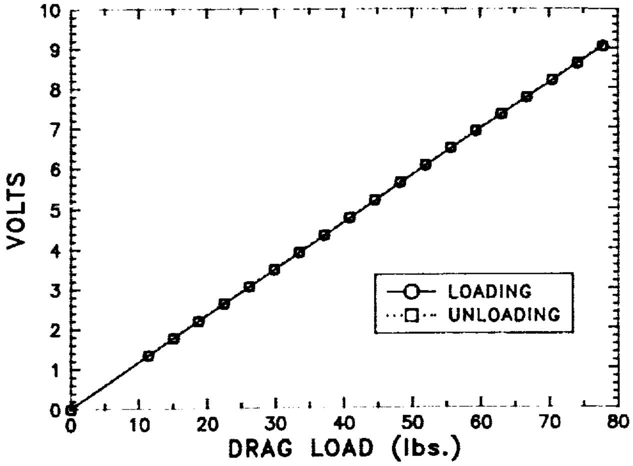

Fig. 18 Drag Calibration

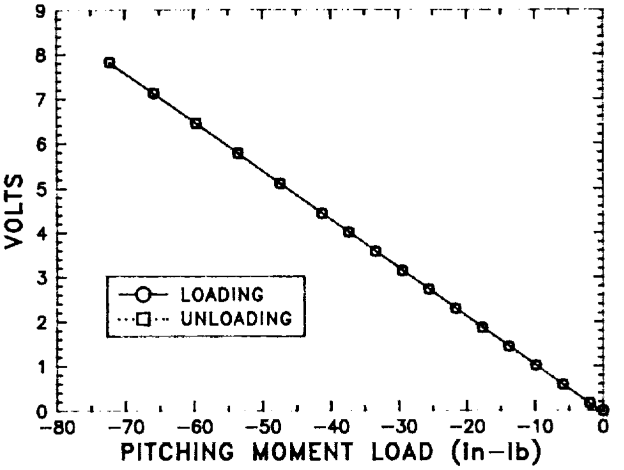

Fig. 19 Pitching Moment Calibration

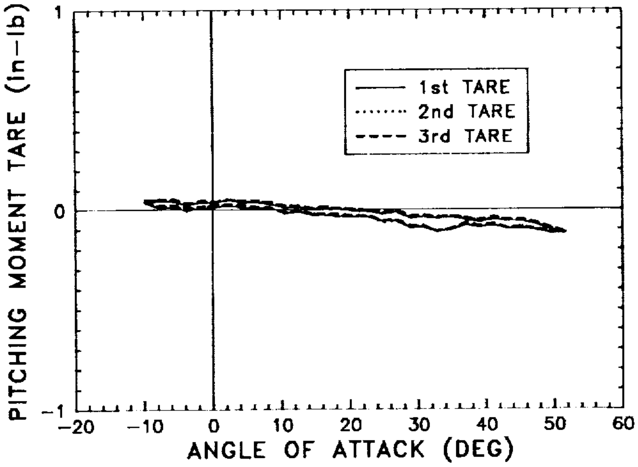

Fig. 20 Pitching Moment Tare Without a Wing (Magnified Scale)

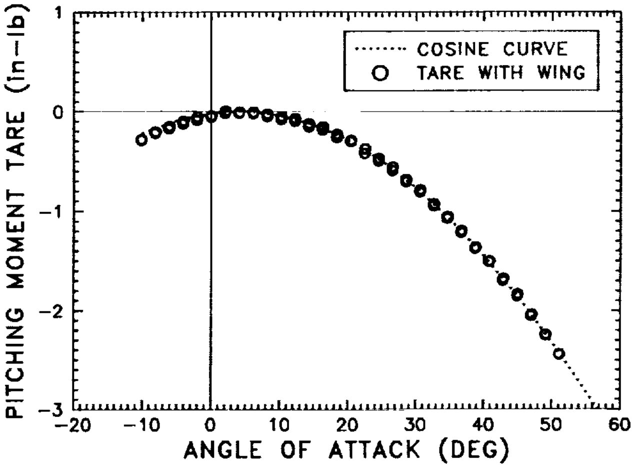

Fig. 21 Pitching Moment Tare with a Wing

NOTES